Sendai virus-based immunoadjuvant in hydrogel vaccine intensity-modulated dendritic cells activation for suppressing tumorigenesis

Bin Zheng [a,*,1], Wenchang Peng [a,1], Lin Gan [b], Mingming Guo [a], Shuchao Wang [a], Xiao-Dong Zhang [a], Dong Ming [a,b,**]

[a] Academy of Medical Engineering and Translational Medicine, Tianjin Key Laboratory of Brain Science and Neural Engineering, Tianjin University, 92 Weijin Road, Nankai District, Tianjin, 300072, China
[b] School of Precision Instrument and Opto-electronics Engineering, Tianjin University, Tianjin, 300072, China

ARTICLE INFO

ABSTRACT

The conventional immunoadjuvants in vaccine have weak effect on stimulating antigen presentation and activating anti-tumor immunity. Unexpectedly, we discovered that non-pathogenic Sendai virus (SeV) could activate antigen-presenting cells (APCs) represented by dendritic cells (DCs). Here, we designed an injectable SeV-based hydrogel vaccine (SHV) to execute multi-channel recruitment and stimulation of DCs for boosting the specific immune response against tumors. After the release of the NIR-triggered antigens from tumor cells, dendritic cells around the vaccine efficiently transport the antigens to lymph nodes and present them to T lymphocytes, thereby inducing systemic anti-tumor immune memory. Our findings demonstrated that the SHV with excellent universality, convenience and flexibility has achieved better immune protection effects in inhibiting the occurrence of melanoma and breast cancer. In conclusion, the SHV system might serve as the next generation of personalized anti-tumor vaccines with enhanced features over standard vaccination regimens, and represented an alternative way to suppress tumorigenesis.

1. Introduction

Cancer is a disease with high morbidity and fatality rate. Anti-tumor vaccine, as everyone knows, is one of the effective means to prevent and suppress tumor occurrence as an artificial initiative immune way [1,2]. Therefore, the research of anti-tumor vaccine has become the focus of many researchers [3–7]. At present, there are mainly two types of anti-tumor vaccines. One is to extract tumor antigens from tumor cells/tissues in vitro or express them in large quantities by means of genetic engineering, and then to generate anti-tumor vaccines by wrapping tumor antigens and immune adjuvants [8–10]. The other is gene recombinant vaccine, which is prepared by inserting tumor antigen gene into virus vector, plasmid or mRNA [11–14]. Although these vaccines can induce immune response and inhibit tumor growth to some extent,

the immune targets of these scheme are single, the immunogenicity is week and the immunoprotective effect is severely limited.

Adjuvant is a nonspecific immuno-agonist, and plays an important role in the vaccine. When it is injected together with antigen or separately in advance, it can enhance the immune response to the antigen or transform the type of immune response [15,16]. Adjuvants can further enhance the expansion ability of immune response, which may be due to changing the physical form of antigen, improving the efficiency of antigen presentation by dendritic cells, or stimulating lymphocyte differentiation [17–19]. There are many kinds of adjuvants for immune activation, such as aluminum hydroxide, lipopolysaccharide (LPS), cytokines, alum, etc. [20–23]. The anti-tumor immunity mainly presents tumor antigens to mature cytotoxic T lymphocyte cells (CTLs) through dendritic cells (DCs), and finally induces the systemic anti-tumor

cellular immune response. Therefore, the development of the immune adjuvants to efficiently stimulate DCs is the key to the preparation of highly effective anti-tumor vaccine.

Microbial-mediated immunotherapy is a promising new direction in the field of tumor therapy [24]. However, some harmful components in bacteria are difficult to completely remove, such as lipopolysaccharide, which may cause fever, shock or other adverse consequences [25]. As the smallest microorganism, virus has a simple structure and strict specificity for host cells, which ensures its safety [26]. Oncolytic viruses [27–29], adenoviruses [30] and lentiviruses [31] have been successfully used in the prevention and treatment of cancer in a large number of experiments and applications. For instance, siRNA and CRISPR/Cas9 gene modification can be used to introduce and express immune-stimulating genes to activate the immune system and prevent the growth of cancer cells [32,33]. However, nucleic acid vaccines and gene therapy methods based on viral vectors not only have complex structures, but also have the carcinogenic risk by integrating the viral genome into the subject's genome [34]. Undoubtedly, natural non-pathogenic viruses with immunomodulatory effects are a better choice in immunotherapy. Sendai virus (SeV) is a type I parainfluenza virus type B, which has no pathogenic to humans. It is usually used as an immune adjuvant in natural immune pathways to achieve functions similar to poly (I:C) and CpG [35,36]. Here, we accidently discovered that SeV can also strongly activate the immune response of DCs, and act as a potential natural adjuvant for DCs activation. However, we also found that free SeV can cause severe blood coagulation reaction, which limits its use in the body.

Notably, the conventional vaccines are usually made from single tumor antigen, which easily leads to immunologic escape. Tumor cells have high adaptability to adverse environments through a variety of cellular mechanisms, such as no or low expression of the previously inoculated tumor antigen to escape the attack of the immune system [37, 38]. Therefore, we speculate that if the whole tumor cells are used as immune vaccination antigen, immunologic escape may be prevented. Since they have all the antigenic components of the tumor cells, the anti-tumor immune response can be excited in multiple ways at the same time, so as to prevent the protective effect of the vaccine from weakening due to the down-regulation of the expression of a single tumor antigen. In addition, we accidently found that when tumor cells are incubated with macrophages after photothermal damage, the production of type I interferon can be detected. We speculate that this may be due to the broken DNA fragmented from the tumor cells produced by thermal damage, which excite STING signaling pathway through phagocytosis of macrophages [39,40].

Based on the above considerations, we designed a SeV-based hydrogel vaccine (SHV) (Fig. 1). This novel anti-tumor vaccine uses virus as adjuvant to recruit and activate a large number of DCs, so as to effectively arouse the body's immune system. The tumor cells in the vaccine acted as an "antigen library" and released all antigens under the trigger of near infrared (NIR). These antigens could be efficiently transported to the lymph nodes by DCs around the vaccine and presented to T lymphocytes, thus inducing systemic anti-tumor immune memory. At the same time, the DNA fragments released under NIR radiation can also promote the activation of STING pathway in macrophages to secrete a large number of anti-tumor cytokines and immune exciting factors. In order to immobilized the tumor cells and prevent their random migration before NIR photothermal killing, a highly biocompatible hydrogel with thermo-sensitive properties was used as a vaccine substrate. Moreover, the hydrogel was also used to prevent SeV from causing blood coagulation in order to ensure the safety of the vaccine. Notably, the combination of the SHV and anti-OX40 (CD134) antibody (aOX40), an important immune checkpoint target, can greatly increase the activation ratio of T cells and enhanced the immune memory of antigens in mouse melanoma and breast cancer models [41, 42]. Theoretically, the SHV can use any tumor cell as an "antigen library" to expand its application scope conveniently. In conclusion, the SHV might serve as the next generation of personalized anti-tumor vaccines, which has enhanced features over standard vaccination regimens and represented an alternative way to suppress tumorigenesis.
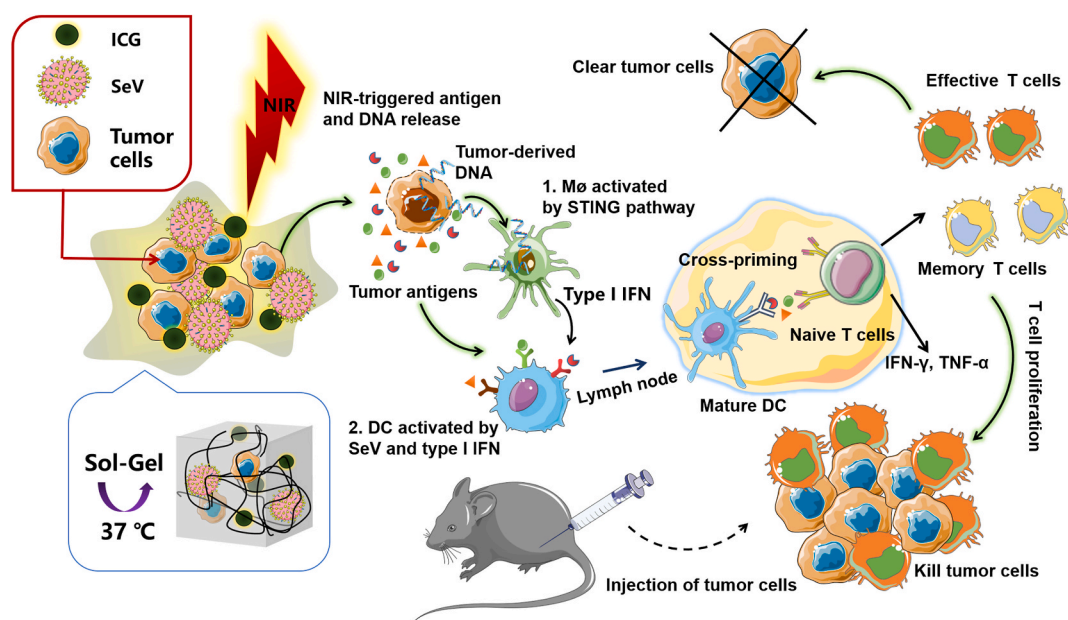
Fig. 1. Schematic diagram of SeV-based hydrogel vaccine (SHV) in preventing tumorigenesis. A highly biocompatible hydrogel as a matrix material was employed to fix tumor cells with temperature sensitivity for supplying all tumor antigens. Photosensitizer (ICG) was used to release tumor antigen precisely under near-infrared laser trigger. Tumor cells ruptured under near-infrared radiation, causing DNA fragmentation to activate STING pathway and secrete type I interferon (IFN). And the Sendai virus (SeV) as an immunoadjuvant efficiently recruited and activated DCs to further activate immunity. DCs then presented tumor antigens to the lymph nodes for maturing T cells and inducing the formation of immune memory cells. When the same tumor cells re-invade, the immune memory cells of mice immunized with the SHV will be efficiently stimulated to kill these invading tumor cells.

2. Materials and methods

2.1. Samples preparation

The Sendai virus (SeV) BB1 strain was donated by Researcher Lishu Zheng from Chinese Center for Disease Control and Prevention (China, CDC). The anti-OX40 antibody (OX40L-Fc (ab221340)) was purchased from Abcam. The monomers D, L-lactide (LA), glycolide (GA) and the initiator poly (ethylene glycol) (Mn 2000 Da) was bought from Sigma-Aldrich Corporation. Stannous octoate was purchased from Sigma and dissolve into anhydrous toluene at 30 mg/mL. The other chemicals were chemical regent grade and bought from Aladdin Corporation. The PLGA-PEG-PLGA triblock copolymers were prepared following typical ring-opening polymerization. Hydroxyl-terminated PEG as the initiator was continuous stirring at 150 °C under vacuum for 4 h, and then LA (0.232 mol) and GA (0.029 mol) with 8/1 M ratio were added and dehydrated under the protection of argon at 80 °C for 3 h. After all the monomers melted, the initiator, 0.2 wt % stannous octoate was added, the mixture was stirred at 150 °C for 12 h. The unreacted monomers and toluene were removed under vacuum at 120 °C for 2 h. The crude product was washed three times with 80 °C water and lyophilized, and the final product was stored at −20 °C. Next, take a certain amount of SeV, ICG, B16/4T1 cells and aOX-40 antibody and mix with the PLGA-PEG-PLGA solution. The mixing components were dissolved completely in ultrapure water to guarantee the molecular-level mixing.

2.2. Samples characterization

The ^{1}H NMR spectrum was recorded in a VARIAN spectrometer (VARIAN INOVA 500 MHz). The sample was dissolved in CDCl$_3$ at concentration 5 mg/mL. Tetramethylsilane was used as the internal reference. The micelle sizes in dilute copolymer aqueous solution were measured in a laser light scattering instrument (Zetasizer Nano ZS90. Malvern). The solutions were filtered through a 0.45 μm filter and equilibrated at each temperature for 15 min before measurement. The TEM experiments were carried out in a JEOL electron microscope (JEM100CXII). In sample preparation, an ultrathin carbon network was dipped in 1 wt% copolymer aqueous solution. The SEM experiments were carried out in a FEI electron microscope (Nanosem 430). In sample preparation, drop the sample on a smooth silicon wafer and heat to 37 °C to make it gel and then immediately transferred to liquid nitrogen and freeze-drying, then sprayed gold on the sample. Sol-gel transition of copolymer aqueous solutions was detected by MCR 702 MultiDrive. Fluorescence absorption curves and fluorescence emission curves of ICG solutions were detected by Thermo Scientific Lumina. Photothermal curve and infrared thermal imaging of ICG solutions (80 μg/ml) under NIR irradiation were detected by FLUKE Ti480 PRO.

2.3. Flow cytometry analysis of activated antigen-presenting cells (APCs)

BD Accuri 6 plus (BD Biosciences) was used for flow cytometry analysis. And we analyzed the results by FlowJo software. Epitope-specific T cells were studied using FITC anti-CD3, APC anti-CD8a and Percp Cy5.5 anti-CD4. Other antibodies used included the following: FITC anti-CD80 (104705, Biolegend), APC anti-CD86 (105011, Biolegend), PE anti-CD62L (104407, Biolegend), APC anti-CD44 (103011, Biolegend), FITC anti-CD103 (121419, Biolegend), PE anti-CD138 (142503, Biolegend), FITC anti-CD45 (103107 Biolegend), PE anti-CD11c (117307, Biolegend). All staining procedures were performed according to the manufacturer's recommendations.

2.4. Animal experiments

To evaluate the *in vivo* immune stimulation of the vaccine, BALB/c female mice (6–8 weeks, SPF level) and C57BL/6 female mice (6–8 weeks, SPF level) were purchased from Huafukang, China, and maintained on standard mouse food and water for 3 days. These C57BL/6 mice were divided into 6 groups, each group consisted of five mice. The experimental mice were immunized twice and the injection site was irradiated with NIR on the second day after vaccination to release tumor antigens. Then inoculated immunized mice with 1.0×10^6 B16 cells. Three days after inoculation with tumor cells, the mice were dissected to check the immune activation *in vivo*. The length (L) and width (W) of each tumor were measured every 2 days with a digital caliper, and the tumor volume was calculated using the formula: tumor volume = (Width^2 × Length)/2. Mice were sacrificed by cervical decapitation 20 days after treatment. Tumors were fixed for immunohistochemistry staining. Similar experiments were performed in BALB/c mice. All the animal experiments involved in this work were approved by the Animal Ethics Committee of Tianjin University.

### 2.5. Mouse specific antibody IgG detection

We used indirect ELISA to detect mouse specific antibody IgG. The ELISA plate was coated with 1 μg/mL B16 or 4T1 cell membrane protein, 100 μL per well, overnight at 4 °C. Cell membrane protein was extracted by Membrane Protein Extraction Kit (K268-50) from Biovision. Diluted the blood supernatant, peritoneal fluid, tumor tissue fluid and spleen cell supernatant of each group of mice to different multiples, then added HRP-marked detection antibody and incubated for 1 h at room temperature. After washing with PBS (pH = 7.4) for 6 times, added 100 μl TMB solutions to each well and incubated in dark for 5–30 min. Finally, 100 μl termination solution was added to each well, and the color changed from blue to yellow. The absorbance at 450 nm was measured within 30 min by microplate. If it was more than 2.1 times of the optical density value of the negative control, it was considered as positive.

3. Results and discussion

3.1. The activating effect of Sendai virus (SeV) on DC cells

As a type B parainfluenza virus, Sendai virus (SeV) has been used as an immune adjuvant in previous reports [43]. According to reports, SeV induces the production of interferon by boosting the TLR7/8 and TLR3 signaling pathways, leading to antiviral immune responses (Fig. 2a) [44, 45]. We occasionally discovered in our experiments that SeV could also activate antigen-presenting cells (APCs), such as dendritic cells (DCs). As shown in Fig. 2b, after 24 h of co-incubation of bone marrow-derived dendritic cells (BMDCs) with 400 UT/ml SeV, the expression of phosphorylated IRF3 and IRF7 proteins also increased significantly. Next, we verified that SeV could induce interferon-β (IFN-β) expression by dual luciferase reporter assay system (Fig. 2c). The levels of tumor necrosis factor-α (TNF-α) (Fig. 2d) and interleukin-6 (IL-6) (Fig. 2e) secreted by BMDCs were up-regulated after SeV stimulation for 24 h. The expression of TNF-α (Fig. S1) and IL-6 (Fig. S2) also increased in the supernatant of DC 2.4 cells stimulated by SeV at a concentration of 400 UT/ml. All the above results indicated that SeV could activate DCs through TLR7/8 and TLR3 signaling pathways, and SeV might be used as a potential agonist of DCs. In addition, we checked the ratio of mature BMDCs by flow cytometry (Fig. 2f and Fig. S3). Under the stimulation of SeV, the expression of costimulatory molecule CD80 increased significantly. From the results of immunofluorescence staining of BMDCs, the expression of costimulatory molecule CD86 was also significantly increased after SeV stimulation (Fig. S4). These results indicated that SeV has the ability to promote the activation and maturation of DCs. Based on the above results, the concentration of SeV used in subsequent experiments was 400 TU/ml.

We speculated that the strong immune activation effect of SeV may be due to its complex structure with single-stranded negative stranded RNA, surface glycoproteins HN and F, and three encoding nucleocapsid proteins NP, P and L [46]. On the other hand, it has been reported that the surface of SeV contains the binding sites of cell surface receptors,
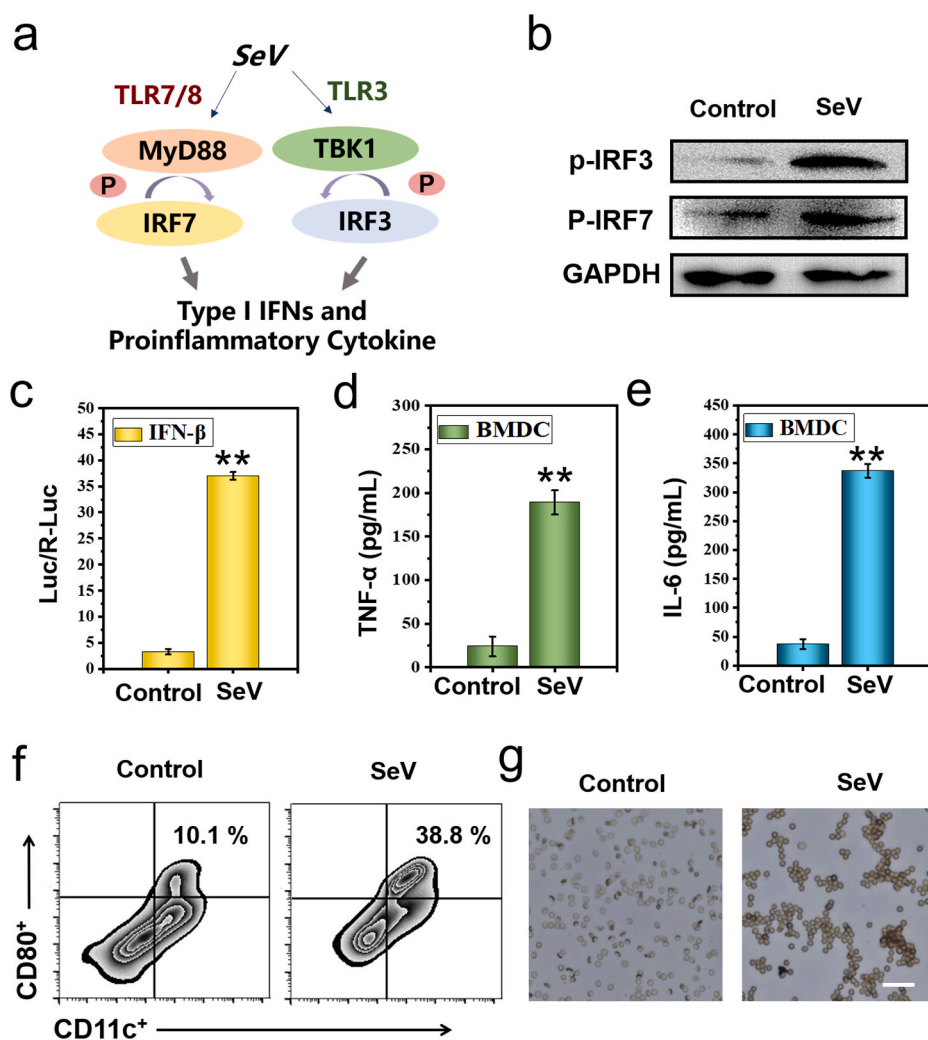
Fig. 2. Sendai virus (SeV) activates dendritic cells through TLR7/8 and TLR3 signaling pathway. (a) Schematic diagram of SeV activated immune signaling pathway. (b) Phosphorylated IRF3 and IRF7 protein expression levels in BMDCs analyzed by western blotting. Experiments were repeated three times. (c)The expression of IFN-β after treatment by SeV. Construct IFN-β-Luc plasmid and co-transfect it with Ren vector into HEK293T cells. Give different treatments for 24 h, and use Promega E5311 microplate reader for detection. (d, e) Secretion levels of TNF-α (d) and IL-6 (e) in BMDCs after 24 h of treatment. (f) BMDCs maturation after treatment by SeV. CD80 and CD11c as markers stained with Percp Cy5.5 anti-CD80 and APC anti-CD11c, respectively. (g) Incubate fresh blood from mice with different materials for 10 min to observe the coagulation of red blood cells. Scale bars, 40 μm. Statistical significance was calculated via one-way ANOVA with a Tukey post-hoc test (c, d and e), *$P < 0.05$; **$P < 0.01$; ***$P < 0.001$.

which can promote the aggregation of different cells, and finally make the cell membranes fuse with each other [47,48]. We incubated SeV with fresh mouse red blood cells to check the safety of the virus. As shown in Fig. 2g, the addition of SeV caused agglutination of red blood cells, which may be harmful to health, thus limiting the use of SeV in the body. Therefore, we consider using a material to wrap the capsid of SeV without changing its immune activation ability.

3.2. Generation and characterization of SeV-based hydrogel vaccine (SHV)

Inspired by the above conclusions, we designed a SeV-based hydrogel vaccine (SHV) consisting of SeV, tumor cells, photosensitizer and temperature sensitive hydrogel. As an immune activator, SeV is used for immune activation of vaccine, recruitment and activation of DCs to improve the efficiency of antigen expression. The tumor cells acted as an "antigen library " and released all antigens triggered by near infrared (NIR). The thermo-sensitive hydrogel has the function of fixing tumor cells and preventing coagulation caused by SeV, endowing the vaccine with injectable property, and ensuring the safety of SHV.

We synthesized a thermo-sensitive biocompatible hydrogel (PLGA-PEG-PLGA) as an important substrate for injectable vaccine. The structures of PLGA-PEG-PLGA used in the scheme were verified by ^{1}H NMR (Fig. 3a). The characteristic peaks of PLGA-PEG-PLGA matched well with the expected chemical shifts. Next, we measured the relationship between the concentration of PLGA-PEG-PLGA and the phase transition temperature by bottle inversion method. As shown in Fig. S5, the low concentration PLGA-PEG-PLGA solution was still liquid at 35 °C. At 35–37 °C (physiological temperature range), 20 wt% PLGA-PEG-PLGA solution transformed from a liquid state into a solid state (Fig. 3b), so 20 wt% PLGA-PEG-PLGA solution was used in the following experiments. Transmission electron microscope (TEM) images showed that the hydrogel was micelles with a diameter of 50–150 nm at 25 °C (Fig. 3c). Surface morphology of temperature sensitive hydrogel in the solid state at 37 °C were observed by scanning electron microscope (SEM), indicating that the hydrogel has undergone phase transformation (Fig. 3d). This phenomenon is due to the formation of hydrogen bonds between polymer chains and water molecules at low temperature, some polymers spontaneously form micelles with hydrophobic PLGA as the core and hydrophilic PEG as the shell, maintaining the equilibrium of PLGA-PEG-PLGA polymer solution system; when the temperature increases, the hydrogen bond between PEG segments and water molecules weakens, the number of micelles in the solution increases and aggregates, leading to the aggregation of PLGA segments hydrophobic interaction becomes the main force of the system, and the sol-gel transformation takes place. Next, we measured the particle size of PLGA-PEG-PLGA micelle by dynamic light scattering (DLS). As shown in Fig. 3e, the micelles particle size was positively correlated with temperature, which further proved the occurrence of micelle aggregation when the temperature increases. In addition, the zeta potential of PLGA-PEG-PLGA solution remained almost neutral (Fig. S6). The sol-gel transition temperature of 20 wt% PLGA-PEG-PLGA solution was 32–35 °C. The addition of other
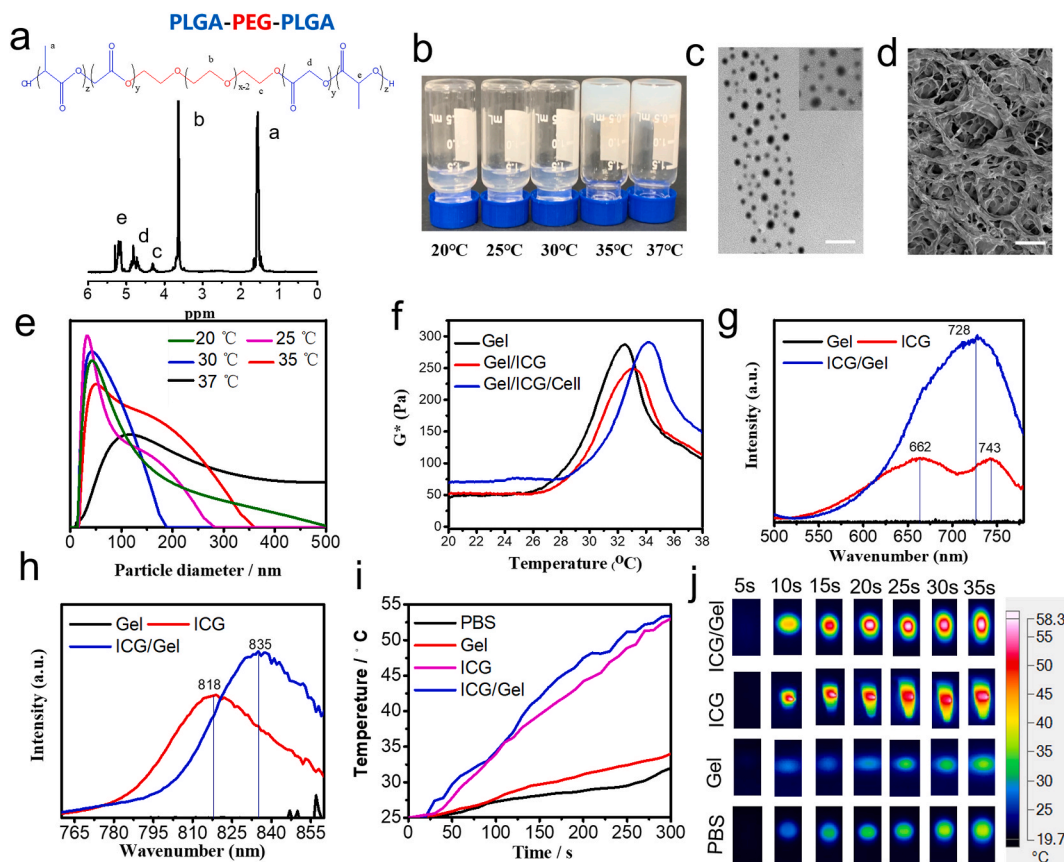
Fig. 3. Characterization of SHV. (a) ^{1}H NMR spectrum of PLGA−PEG−PLGA triblock copolymer in CDCl$_3$. (b) Representative photographs of the 20 wt% copolymer system at the indicated temperature. Experiments were repeated three times. (c) Transmission electron microscopy (TEM) images of hydrogel's nano micelle at 25 °C. Scale bars, 500 nm. (d) Representative cryo-scanning electron microscope (SEM) images of hydrogel at 37 °C. Scale bars, 50 μm. (e) Micellar particle size curves of PLGA-PEG-PLGA at different temperatures. (f) Sol-gel transition of copolymer aqueous solutions. (g) Fluorescence absorption curves of ICG solutions. (h) Fluorescence emission curves of ICG solutions. (i, j) Photothermal curve (i) and infrared thermal imaging (j) of ICG solutions (80 μg/ml) under NIR irradiation (808 nm, 100 mW/cm^2).

components in the vaccine system did not change the phase transition temperature of PLGA-PEG-PLGA (Fig. 3f). Its temperature sensitivity ensured that it can be injected at room temperature and undergo sol-gel transition *in vivo* to immobilized tumor cells, photosensitizers and SeV under the skin. In order to verify the biocompatibility of the gel, we co-cultured it with dendritic cells for 24 h, and then checked the cell viability by staining with dead and live cells (Fig. S7) and MTT test (Fig. S8). Compared with the control group, the PLGA-PEG-PLGA gel had no obvious effect on the viability of dendritic cells, indicating that it had good biocompatibility. The above results confirmed that PLGA-PEG-PLGA gel has the characteristics of temperature-sensitive phase-change, and can be used to fix SeV and tumor antigens in the body to ensure the safe use of SHV.

Then, we verified the role of photosensitizer indocyanine green (ICG) in SHV system *in vitro* for damaging tumor cells to promote the NIR-triggered release of tumor antigens. As shown in Fig. 3g and h, the fluorescence absorption peak of ICG is at 662 nm and 743 nm, and its fluorescence emission peak is at 818 nm. The absorption peaks and emission peaks of ICG/Gel are located at 728 nm and 835 nm respectively. (Fig. 3g and h). These results indicated that NIR can stimulate ICG and control the precise release of tumor antigen. As shown in Fig. S9, under NIR irradiation, the temperature of 0.2 mg/ml ICG solution increased to about 50 °C within 10 min. When the temperature of the hydrogel reached 50 °C, the cancer cells in it would be thermally damaged and decomposed. Therefore, we used 0.2 mg/ml ICG in subsequent experiments. In order to monitor the photothermal effect of ICG *in vitro*, the infrared thermal images and temperature change of ICG

solution irradiated by NIR were recorded simultaneously by infrared thermograph (Fig. 3i and j). The temperature change of each group showed that ICG/Gel had better photothermal effect than PBS and single hydrogel. Therefore, the above results indicated that the tumor cells in the SHV could be destroyed to release antigens accurately under the trigger of NIR.

3.3. Verification of immune activation performance of tumor cells destroyed by NIR

After successfully characterizing the characteristics of hydrogel and ICG in vaccine, we investigated the performance of NIR-triggered tumor antigens release. B16 cells were incubated with gel, ICG and ICG/Gel, and irradiated by NIR for 10 min. As shown in Fig. 4a, the cell damage of ICG/Gel was negligible without the near infrared irradiation, which further proved the biocompatibility of the hydrogel vaccine. In addition, the irradiation of NIR alone had little effect on cell survival. However, B16 cells treated by ICG and ICG/Gel with NIR irradiation showed a huge amount of red fluorescence due to the severe cellular damage caused by photothermy. These results demonstrated that ICG/Gel could destroy tumor cells by NIR. Meanwhile, B16 cells in the hydrogel after being irradiated by NIR were taken out for separation and analysis by flow cytometry (Fig. S10). The results revealed that the photothermal effect triggered by NIR could significantly induce tumor cell apoptosis to precisely release tumor antigens from the SHV. At present, for the production of tumor vaccines, the methods for extracting all tumor antigens mainly include freeze-thaw method and ultrasonic destruction method.
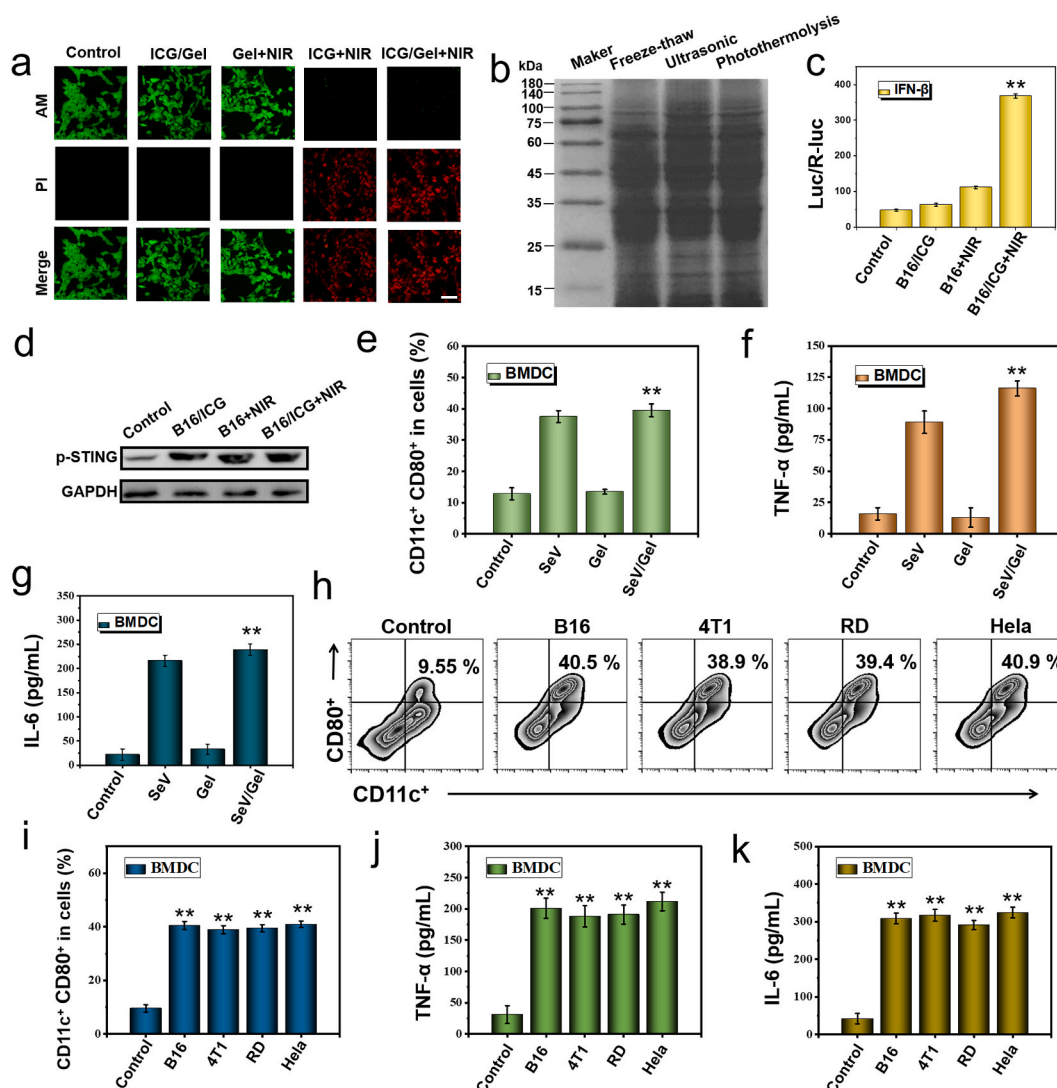
Fig. 4. Verification of immune excitation performance of SHV *in vitro*. (a) Live/dead cell staining of B16 cells treated with ICG/Gel (1 μM ICG) under NIR irradiation (808 nm, 100 mW/cm^2, 10 min). Live cells (green) and dead cells (red) were stained with Calcein AM and propidium iodide (PI), respectively. Scale bars, 60 μm. (b) The antigen proteins were obtained by freeze-thaw, ultrasonic and photothermolysis. Coomassie brilliant blue staining of SDS-PAGE. (c) The expression of IFN-β after different treatment. Construct IFN-β-Luc plasmid and co-transfect it with Ren vector into HEK293T cells. Give different treatments for 24 h, and use Promega E5311 microplate reader for detection. (d) Phosphorylated STING protein expression levels in RAW 264.7 cells analyzed by western blotting. Experiments were repeated three times. (e) Activated DC ratio of BMDCs after different treatment. CD80 and CD11c as markers stained with Percp Cy5.5 anti-CD80 and APC anti-CD11c, respectively. (f, g) Secretion levels of TNF-α (f) and IL-6 (g) in BMDCs. (h) The mature DCs of BMDC treated with vaccines containing different cancer cells as antigens. CD80 and CD11c as markers stained with Percp Cy5.5 anti-CD80 and APC anti-CD11c, respectively. (i) Activated DC ratio of (h). (j, k) Secretion levels of TNF-α (j) and IL-6 (k) in BMDCs treated with vaccines containing different cancer cells as antigens. Statistical significance was calculated via one-way ANOVA with a Tukey post-hoc test (c, f, g, h and i), *P < 0.05; **P < 0.01; ***P < 0.001.

Therefore, we compared the antigen released by NIR irradiation with that extracted by freeze-thaw method and ultrasonic method (Fig. 4b). The location of protein bands of tumor antigen extracted by three methods was basically the same, which indicated that all tumor antigens can be released through NIR mediation.

We found out by accident that the residual DNA fragment could activate the phosphorylation of STING protein (stimulator of interferon genes), which phosphorylation of STING protein was a key link in the excitation of cGAS-cGAMP-STING signaling pathway [49]. In natural, tumor cells escaped immune response by inactivating STING signaling pathway of APCs. However, the residual DNA fragments induced by NIR irradiation could arouse STING signaling pathway of macrophages, similar to that of the activator such as cGAMP. We analyzed the expression level of phosphorylated STING protein in RAW 264.7 cells by western blotting and quantitatively analyzed the expression of STING protein and internal reference protein by Image J (Fig. 4d, S11 and S12).

The relative expression of p-STING protein in ICG/Gel group was the highest under NIR irradiation (Fig. S13). Next, we checked the production of IFN-β after 24 h of different treatment through the dual luciferase reporter system (Fig. 4c). The expression of IFN-β increased significantly in ICG/Gel group. These results further confirmed that the residual DNA fragments could activate STING signaling pathway and induce anti-tumor response.

3.4. In vitro immune activation performance of SHV

As an attenuated strain, SeV would not cause serious diseases *in vivo*, but its biological safety must be carefully evaluated before use. When the free virus was incubated with fresh red blood cells of mice for 10 min, the red blood cells gathered obviously. Because the hemagglutinin neuraminidase (HN) on the surface of the virus stimulated the coagulation factors of red blood cells and then triggered the cascade of

agglutination reactions. While the virus was encapsulated into the hydrogel vaccine, there was almost no aggregation of red blood cells (Fig. S14). The above phenomenon indicates that SeV did not cause red blood cell agglutination after hydrogel treatment to ensures the safety of virus use.

In addition, we checked the stimulated immune responses of APCs by the SHV *in vitro*. It has been reported that the activation of anti-tumor immune responses would be accompanied by the maturation of DCs and the production of relevant cytokines (such as TNF-α and IL-6) [50–52]. The BMDCs were collected after being treated with different groups for 48 h. And the proportion of matured DCs (CD80$^+$, CD11c$^+$) was detected by fluorescence activating cell sorter (FACS) (Fig. 4e and Fig. S15). The percentage of mature DCs in group SeV/gel increased significantly, indicating that SHV had immunological stimulatory effect. After SeV/gel treatment for 24 h, we detected the increase of two typical cytokines TNF-α (Fig. 4f) and IL-6 (Fig. 4g) in the cell supernatant. After the same treatment in macrophages (another important APC), the secretion level of TNF-α also increased significantly (Fig. S16). As expected, SeV/Gel resulted in higher cytokine release than the control group, demonstrating that SeV and hydrogel mixture effectively stimulate immune response.

Subsequently, we verified the activation effect of the SHV on dendritic cells. We selected mouse melanoma cells (B16), mouse breast cancer cell (4T1), human cervical cancer cell (HeLa) and human malignant embryonic rhabdomyoma cell (RD) as vaccine antigens respectively. The cancer cells were mixed with other components of the vaccine and irradiated by NIR for 10 min. After co-cultivating the prepared vaccine with BMDCs for 24 h, the proportion of mature DCs was checked by flow cytometry (Fig. 4h and i). Compared with the control group, the DC maturation ratio of each vaccine group was greatly increased. The secretion level of immune cytokines was also greatly increased in the vaccine group, including TNF-α and IL-6 (Fig. 4j and k). These results all show that SHV system is universal and can activate dendritic cells under the cooperation of different antigens.

3.5. Immune excitation in vivo of SHV

After vaccination, the type and quantity of immune cells and cytokines will change greatly. Prompted by the promising *in vitro* results, we proceeded to study the *in vivo* immunostimulatory effects for C57BL/6 mice (6–8 weeks) after different treatment. According to the experimental results *in vitro*, the SHV consisted of 400 Tu/ml SeV, 0.2 mg/ml ICG and 20 wt% PLGA-PEG-PLGA. Melanoma B16 cell line has the advantages of high tumor formation rate and convenient observation and measurement in C57BL/6 mice. Therefore, we used B16 cells as vaccine antigen model. Next, we discussed the amount of B16 cells used in the SHV. As shown in Fig. S17, no tumor formation was observed in mice injected with 1×10^3 B16 cells in the hydrogel vaccine. On the contrary, 1×10^6 B16 cells could form obvious tumor within 7 days after subcutaneous injection. In order to fully ensure the safety of the vaccine, we used 1×10^3 B16 cells as the SHV dose. And 1×10^6 cells were used as the amount of inoculation to verify the effect of the vaccine.

In addition, we combined the SHV with anti-OX40 antibody (aOX40) to enhance the efficacy of the vaccine. According to the previous report, 50 μg aOX40 per mouse has been shown to have an extremely desirable immune-activating effect [53,54]. Binding with OX40 ligand on the surface of T cells by aOX40 can greatly improve the survival and expansion of effector T cells and memory T cells, and reduce the immunosuppressive viability of Tregs, and stimulate the secretion of cytokines (such as IFN-γ) to further amplify the T cell excitation effect and enhance the immune memory effect of the antigen [53,55]. In order to verify the activation effect of aOX40 on T cells, we injected aOX40 into C57BL/6 mice and examined the activation of T cells in spleen three days later. After aOX40 treatment, the activation ratio of CD4$^+$ T and CD8$^+$ T cells was significantly increased (Fig. S18). The results show that aOX40 is effective for activating helper T cells and cytotoxic T

lymphocytes, and may enhance the immune effect of the vaccine.

As shown in Fig. 5a, the experimental mice were immunized twice and then inoculated with B16 cells. There was an obvious prominence of the subcutaneous injection site (red circle part) after the SHV vaccination (Fig. 5b). At this time, SeV in the SHV recruited and activated the surrounding DCs. On the second day, NIR was used to irradiate the prominence and release the tumor antigen. To monitor the photothermal effects of ICG *in vivo*, the infrared thermographic maps were recorded by an infrared thermal imaging camera (Fig. 5d). The SHV had excellent photothermal effect, which could destroy tumor cells for releasing tumor antigens. Then, we extracted the vaccine injection area tissue, tumor tissue and normal subcutaneous tissue for protein analysis. The protein band of the vaccine tissue was basically the same as that of the tumor tissue, which proved that the vaccine could release all tumor antigens after NIR irradiation (Fig. 5c).

After twice immunization, C57BL/6 mice were subcutaneously inoculated with 1.0×10^6 B16 cells to verify the immune protection of the SHV *in vivo*. Three days after inoculation of B16 cells, various types of immune cells and cytokines in interstitial fluid, lymph nodes, peritoneal fluid, spleen and blood were analyzed by flow cytometry and ELISA (Fig. 5e and f). APCs are the most important immune cells for recognition and presentation of antigenic peptides. After immunization with SHV, we gave priority to monitoring the activation of APCs. After immunization and tumor inoculation in the middle and upper groin of mice, we examined the activation of DCs in inguinal lymph nodes. After injection of hydrogel vaccine, the expression of typical mature DCs surface marker molecule CD11c$^+$ increased significantly (Fig. 5g). The increasing of maturation DCs in other sites was consistent with the trend in lymph nodes (Figs. S19 and S20). These results indicate that the SHV could efficiently recruit DCs under the stimulation of SeV, and transported these tumor antigens to lymph nodes under the immune enhancement effect of aOX40.

Next, we examined the effect of the SHV on the polarization of T cells in various parts of C57BL/6 mice. CD4$^+$ T cells can not only directly secrete large amounts of cytokines that kill tumor cells and inhibit tumor cell growth and proliferation, but also play an auxiliary role in the stimulation and proliferation of CD8$^+$ T cells, which helps to generate and ensure long-term immunologic memory. Compared with the control group, the percentage of CD4$^+$ T cells in the tissue fluid of the tumor site was significantly increased (Fig. 5h). And the proportion of activated CD8$^+$ T cells was also increased (Fig. 5i). The increase of CD8$^+$ T cells may be due to the local cross presentation of antigen by DCs, which triggers systemic anti-tumor immunity. The differentiation trend of T cells in lymph nodes, peritoneal fluid, spleen and blood of immunized mice was similar (Figs. S21–24). The immune activation of SeV/cell/aOX40/ICG without NIR irradiation was very weak. Without irradiation, the antigens could not be successfully released from tumor cells, which reduced the immune effect of the vaccine. The Cell/aOX40/ICG group and SeV/aOX40/ICG group lacked SeV or tumor antigens and could not activate the immune system. The lack of aOX40 in SeV/Cell/ICG group limited the immune stimulation of the vaccine. The blood samples were taken from each group to detect the secretion levels of IFN-γ (Fig. 5e) and TNF-α (Fig. 5f). As expected, the combination of SHV and aOX40 could enhance the secretion of cytokines, further kill tumor cells and enhance the anti-tumor immune response.

3.6. SHV mediated proliferation and activation of antigen-specific T cells

First, we aseptically isolated the spleen cells of the immunized mice for culture (Fig. S25). We measured the proliferation of spleen-derived lymphocytes stimulated by tumor antigen obtained from photothermal decomposition by MTT assay (Fig. 5j). The results showed that compared with the control group, tumor antigen could induce specific proliferation of lymphocytes, and other components of the vaccine had no effect on cell proliferation. Subsequently, we measured the activation of helper T cells (CD4$^+$) and cytotoxic T lymphocytes (CD8$^+$) after *in*
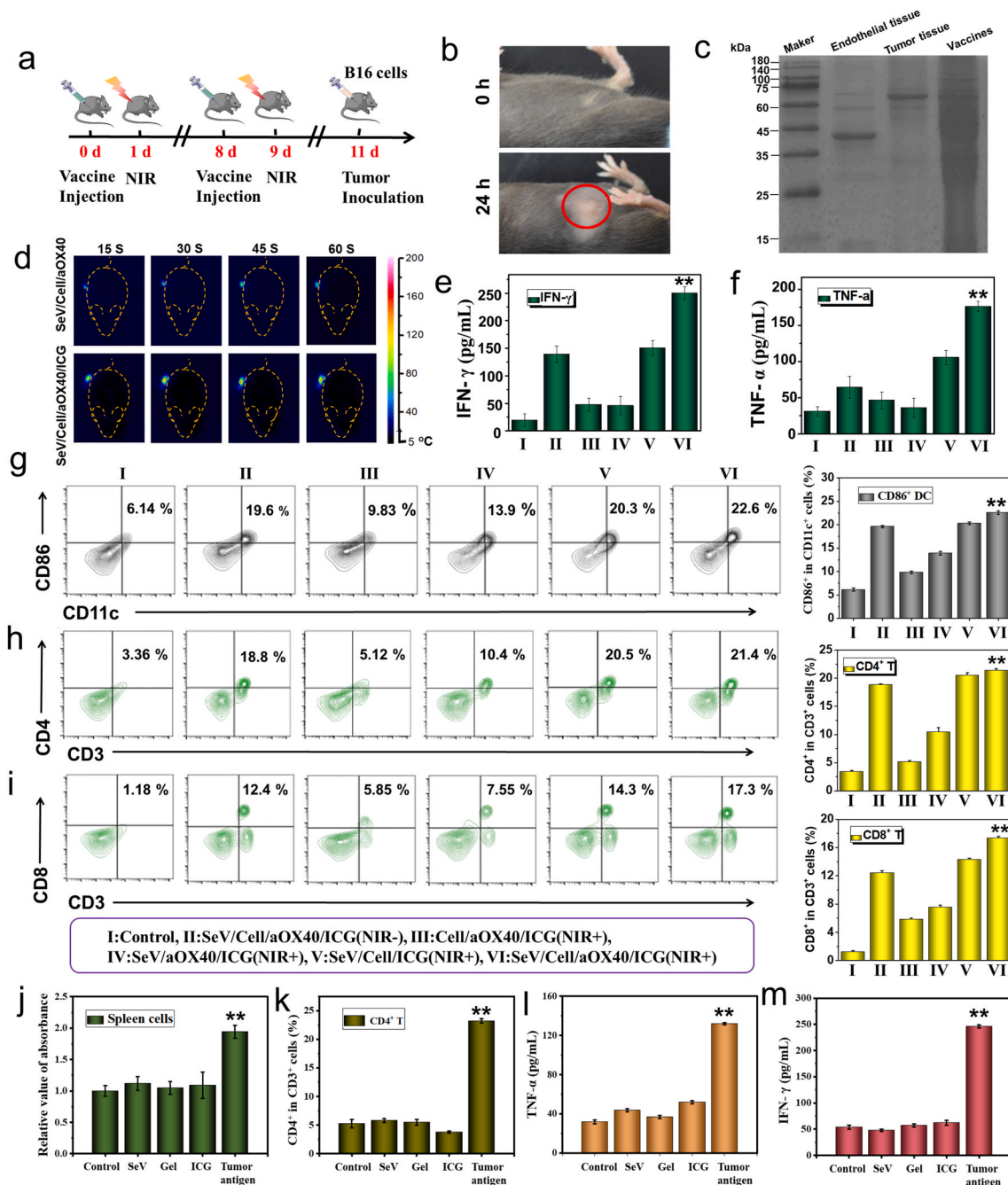
Fig. 5. *In vivo* immune activation effect of SHV. (a) Schematic of various treatment steps for evaluating the tumor immunity efficiencies of different treatment in C57BL/6 mice. (b) Representative photographs of mice before and after vaccine injection. (c) Proteins contained in tumor tissue, normal subcutaneous tissue and subcutaneous vaccine tissue *in vivo*. Coomassie brilliant blue staining of SDS-PAGE. (d) *In vivo* infrared thermal imaging of different groups under the NIR irradiation (808 nm, 100 mW/cm²). Experiments were repeated three times. (e, f) Secretion levels of IFN-γ (e) and TNF-α (f) in the blood from immunized mice. (g) Activated DC ratio in inguinal lymph nodes for mice with different treatment (n = 3). APC anti-CD86 and PE anti-CD11c stained with CD86 and CD11c markers in DCs. (h) Helper T cells in interstitial fluid after treatment (n = 3). CD3 and CD4 as markers on CD4⁺ T cell surfaces stained with Percp Cy5.5 anti-CD4 and FITC anti-CD3. Experiments were repeated three times. (i) Cytotoxic T lymphocytes in interstitial fluid after treatment (n = 3). CD3 and CD8a as markers on CD8⁺ T cell surfaces stained with APC anti-CD8a and FITC anti-CD3. Experiments were repeated three times. (j) *In vitro* proliferation of spleen cells of immunized mice. (k) Helper T cells in spleen cells of immunized mice after different stimulation *in vitro*. CD3 and CD4 as markers on CD4⁺ T cell surfaces stained with Percp Cy5.5 anti-CD4 and FITC anti-CD3. Experiments were repeated three times. (l, m) The secretion levels of IFN-γ (l) and TNF-α (m) in spleen cells of immunized mice after different stimulation *in vitro*. Statistical significance was calculated via one-way ANOVA with a Tukey post-hoc test (g, h, i, j, k, l and m), *P < 0.05; **P < 0.01; ***P < 0.001.

vitro stimulation. Under the stimulation of tumor antigens, the activation ratio of CD4⁺ T and CD8⁺ T cells increased noticeably (Fig. 5k and S26-28). These results further confirmed the antigen specificity of T cell activation. Next, we examined the cytokine secretion of spleen-derived lymphocytes after 12 h of stimulation (Fig. 5l, m). After tumor antigen stimulation, the secretion level of TNF-α and IFN-γ increased

significantly. It was further proved that the SHV activated antigen-specific immunity.

In addition, we also examined the antigen specificity of lymph node derived lymphocytes. We isolated lymphocytes from the inguinal lymph nodes immunized mice for *in vitro* culture, and then re-stimulated them with tumor antigen (Fig. S29). The results showed that lymphocyte

proliferation was rapidly induced after tumor antigen stimulation, while other components of the vaccine did not. These results manifested that lymph node derived lymphocytes proliferated specifically to tumor antigen, but not to other components of vaccine. And revealed that the SHV can trigger systemic specific immune memory to play a crucial role in protecting the body when the same antigen invades again.

3.7. Immune memory and the protective effect of SHV on melanoma

Antibody is a kind of protective immunoglobulin produced by antigen stimulation, which can trigger the specific killing effect of immune system. In order to prove the effectiveness of SHV, we tested the titer of *anti*-B16 IgG in peritoneal fluid (Fig. 6a), spleen (Fig. 6b), blood (Fig. 6c) and interstitial fluid (Fig. 6d) of mice in each group. Compared with the control group, the *anti*-B16 IgG titer of the experimental group after

hydrogel vaccine containing all ingredients treatment increased significantly. Subsequently, we verified the specific binding ability of antibody in serum of immunized mice to B16 cells *in vitro*. We inoculated B16 cells into 96 well plates and then incubated them with PBS, WT or immunized mice serum for 12 h. Next, we detected the antibody bound to the cell surface through the HRP-labeled anti-antibody and the microplate reader. The results show that the antibodies in the mouse serum of immunized mice could bind to the corresponding cell surface, and then activate the immunity to eliminate tumor cells (Fig. S30). This result suggested that specific immunity against the tumor is produced after SHV vaccination.

Antibodies are secreted by plasma cells, also known as effector B cells. Subsequently, the mature effector B cells were detected by flow cytometry. The results showed that the proportion of mature effector B cells in bone marrow increased by more than 10 times after the full
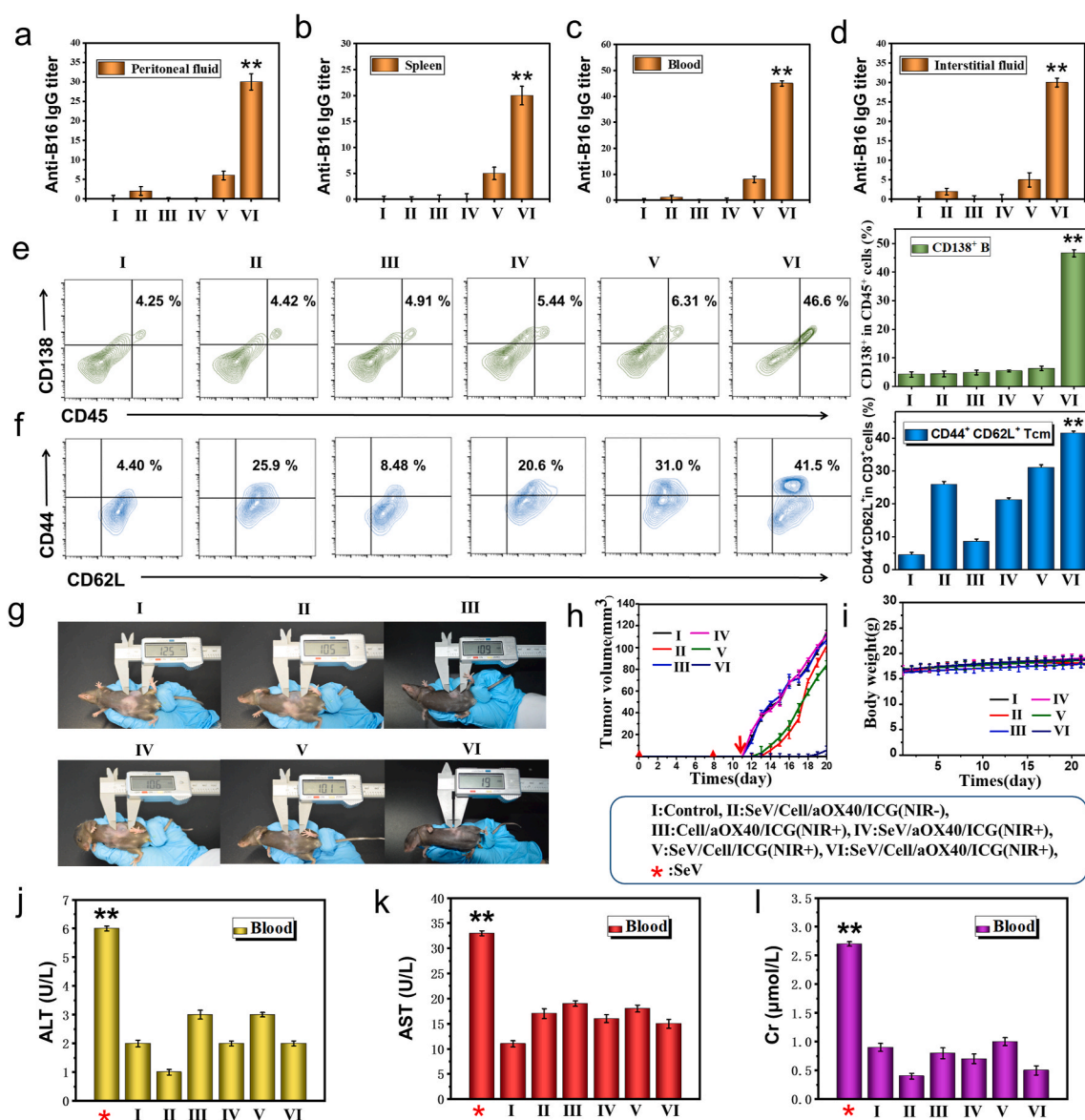
Fig. 6. The immune memory effect of SHV inhibited tumor growth. (a–d) Anti-B16 IgG titer in peritoneal fluid (a), spleen (b), blood (c) and interstitial fluid (d). (e) Activated B cell ratio in bone marrows for mice with different treatment (n = 3). PE anti-CD138 and FITC anti-CD45 stained with CD138 and CD45 markers in B cells. (f) Activated Central Memory T cell ratio in inguinal lymph nodes for mice with different treatment (n = 3). PE anti-CD62L and APC anti-CD44 stained with CD62L and CD44 markers in Tcms. (g) Representative photographs of tumors two weeks after injection of B16 cells in pre-immunized C57BL/6 mice. (h) The growth curve of tumors in C57BL/6 mice. (i) The body weight change curve of B16 tumor-bearing mice during the three weeks evaluation period. (j–l) Compared with mice injected with free SeV, the value of ALT(j), AST(k) and Cr(l) in the blood of mice. Statistical significance was calculated via one-way ANOVA with a Tukey post-hoc test (a, b, c, d, e, f, j, k and l), *P < 0.05; **P < 0.01; ***P < 0.001.

hydrogel vaccine was immunized to C57BL/6 mice (Fig. 6e). In addition, we also checked the activation of B cells in the spleen (Fig. S31). Besides, the cells in the interstitial fluid, blood and lymph nodes were also collected for flow cytometry analysis. The results illustrated that the proportion of mature effector B cells in these sites also increased significantly (Figs. S32 and S33). The results showed that the SHV could effectively stimulate the body's humoral immunity against tumor antigens and improve the therapeutic effect of tumor.

The above studies indicate that SHV can successfully induce the humoral immunity of C57BL/6 mice to efficient killing of tumor cells. As "inspectors", memory T cells can prevent the recurrence of the same tumor after vaccination, which is the most important lymphocyte for long-term prevention of tumor. Central Memory T cells (Tcm) have long-term memory after being activated by an antigen and can home to lymph nodes to receive the same antigen. The activated Tcm can continue to produce a large number of effective memory T cells (Tem) under the stimulation of the same antigen again to perform a super anti-tumor killing effect. Compared with the control, the proportion of CD44$^+$ CD62L$^+$ T cells (the most important marker molecule of Tcm cells) increased significantly in the inguinal lymph nodes after vaccination with hydrogel vaccine containing all ingredients immunization (Figs. 6f and S34). The proportion of Tcm activation in interstitial fluid, peritoneal fluid, spleen and blood also increased (Figs. S35–37). Moreover, the proportion of CD8$^+$ T cells in tumor sections of mice after immune treatment increased (Fig. S38). The results of TUNEL immunohistochemical analysis of tumor sections also showed that the apoptosis of tumor cells in the combined immunotherapy group was the most obvious (Fig. S39). These results indicate that the SHV not only stimulated cellular immunity and humoral immunity, but also promoted the formation of memory cellular immunity to protect the body by rapidly generating specific immune responses when the same antigen invades next time.

The above studies showed that after SHV immunized C57BL/6 mice, corresponding immune memory cells were formed *in vivo*. After inoculation with hydrogel vaccine, C57BL/6 mice were injected with B16 cells subcutaneously. After inoculation with all components of the hydrogel vaccine, the growth of the tumor was significantly inhibited (Fig. 6g and h and S40). Although SeV/Cell/aOX40/ICG and SeV/Cell/ICG/NIR immunization groups had slight inhibitory effect on tumor growth, there was still significant difference compared with SeV/Cell/aOX40/ICG/ NIR group, which had almost no tumor growth. The reason may be that without laser irradiation, the antigen of tumor cells cannot be completely released, greatly reducing the immune protection effect of the vaccine on melanoma. The lack of aOX40 in the vaccine cannot achieve the best effect of activating T cells. The tumor volume of Cell/ aOX40/ICG/NIR and SeV/aOX40/ICG/NIR groups increased rapidly within 10 days, and the growth curve trend was similar to that of PBS group. This may be because vaccines lacking immune activators or antigens are difficult to stimulate the body's immune memory against tumor. These results indicated that the combination of SHV and aOX40 can stimulate the adaptive immune response and effectively enhance the prevention of oncogenesis.

3.8. The downstream pathway of interaction between activated immune cells and cancer cells ex vivo

Next, we analyzed the interaction between activated immune cells and cancer cells using B16 cells as antigen. We isolated spleen-derived lymphocytes from WT mice and immunized mice and cultured them *in vitro*. At the same time, we also isolated subcutaneous tumor cells of WT mice for culture, including B16 and 4T1. After culture of spleen derived lymphocytes and tumor cells for 6 h, and then the apoptosis of tumor cells was detected. Annexin V is a sensitive indicator for detecting early cell apoptosis. We used FITC-labeled annexin V as a fluorescent probe to detect the occurrence of cell apoptosis by flow cytometry (Fig. S41). The spleen-derived lymphocytes of immunized mice and tumor cells co-

incubated group showed obvious apoptosis. However, activated lymphocytes did not induce apoptosis of xenogeneic tumor cells. Next, we examined the rupture of DNA in apoptotic cells by TdT-mediated DUTP nick end labeling (TUNEL) (Fig. S42). The tumor cells treated with PBS and WT lymphocytes were almost not stained, indicating that there was no DNA fragmentation and 3′-OH formation. On the contrary, DNA fragmentation occurred in tumor cells treated with lymphocytes from immunized mice. DNA damage and leakage could also be observed from DAPI staining. The above results confirmed that activated lymphocytes have specific targeted killing activity and induce the apoptosis of tumor cells.

Subsequently, we further studied the downstream pathway of activated immune cells inducing cancer cells apoptosis. After incubating with lymphocytes for 6 h, we quantitatively analyzed the expression of apoptosis related genes by real-time quantitative PCR detecting system (qPCR). Fas associated protein with a novel death domain (FADD) is a kind of Fas related protein in the death domain, which can activate a series of caspase-8, 1, 3, 7 and promote the apoptosis of the cells. The expression of FADD in tumor cells increased significantly after co-incubation with lymphocytes from immunized mice, indicating that Fas apoptotic pathway was activated (Fig. S43). At the same time, the expression of pro-apoptotic P53 and Bax in tumor cells increased significantly, while the expression of anti-apoptotic Bcl2 decreased, which indicated that the P53-Bax mitochondrial apoptotic pathway was also activated. Caspase-3, a common downstream effect of multiple apoptosis pathways, was also activated and initiated DNA degradation (Figs. S44 and S45). Next, we checked the expression levels of cell cycle related genes Cdk2 and Cyclin D1 in each group of cells. After treatment with lymphocytes immunized mice, the expression of Cdk2 and Cyclin D1 of tumor cells were significantly reduced, indicating the occurrence of cell cycle arrest (Fig. S46). These results indicated that activated immune cells can promote tumor cell apoptosis through Fas pathway and P53-Bax pathway, and cause tumor cell cycle arrest (Fig. S47).

3.9. Biological safety of SHV in vivo

Although non-pathogenic SeV has been encapsulated in hydrogel vaccine, the biological safety of its application *in vivo* needs further confirmation. One week after the end of immunization, we extracted the fresh blood of mice in each group and observed under the microscope. The morphology of red blood cells in mice immunized with the vaccine was normal, and there was no aggregation (Fig. S48). Subsequently, we seriously monitored the acute cytokines that usually result from viral infection by ELISA. After subcutaneous injection of free virus, serum alanine aminotransferase (ALT) (Fig. 6J), aspartate aminotransferase (AST) (Fig. 6K) and creatinine (Cr) (Fig. 6L) were significantly increased, suggesting that SeV may cause mild acute infection. Although this infection would not cause obvious disease, it was also not allowed in clinical practice. The SHV did not cause an increase in the expression level of acute infectious factors. After vaccination of C57BL/6 mice, the body weight of all groups did not change obviously, proving that these anti-tumor vaccines have good biocompatibility *in vivo* (Fig. 6i). Two weeks after the end of immunization, the mice were sacrificed and the corresponding tissues were separated for the subsequent analysis. The digital photos of main organs of mice in each group (Fig. S49) and the H&E staining (Fig. S50) of histological sections showed little difference, indicating that the side effects of SHV in main organs were negligible. In conclusion, the SHV had good biological safety and could effectively inhibit the occurrence of melanoma through immunological agonists and tumor antigen release triggered by NIR.

3.10. SHV for systemic antitumor immune response to suppress breast cancer

In order to verify the universality of the SHV system, we studied the immunostimulatory effect of BLAB/c mice against breast cancer. First,

we injected BLAB/c mice with SHV and released the tumor antigen under NIR radiation on the second day. Next, we used flow cytometry to detect the damage of 4T1 cells in thermosensitive hydrogel induced by NIR irradiation. Under NIR irradiation, the late apoptosis of tumor cells in the vaccine group increased nearly three times compared with the control group, resulting in the release of tumor antigen (Fig. 7a). On the third day after immunization, the expression levels of anti-tumor cytokines TNF-α and IFN-γ in blood and body fluid samples of each group increased significantly (Fig. 7b and c). In addition, to further verify the immune activation effect of the vaccine *in vivo* of BLAB/c mice, interstitial fluid, lymph nodes, spleen and blood were collected and analyzed by flow cytometry. As expected, we observed more activated DCs in inguinal lymph nodes for mice after vaccine immunization (Fig. 7d). Compared with the control group, the proportion of CD8$^+$ T cells and CD4$^+$ T cells for executing an anti-tumor cellular immunity were significantly increased in the interstitial fluid after immunization (Fig. 7e, g). The increased proportion of maturation of DCs and T cells indicates that the SHV immunization could initially induce the immune
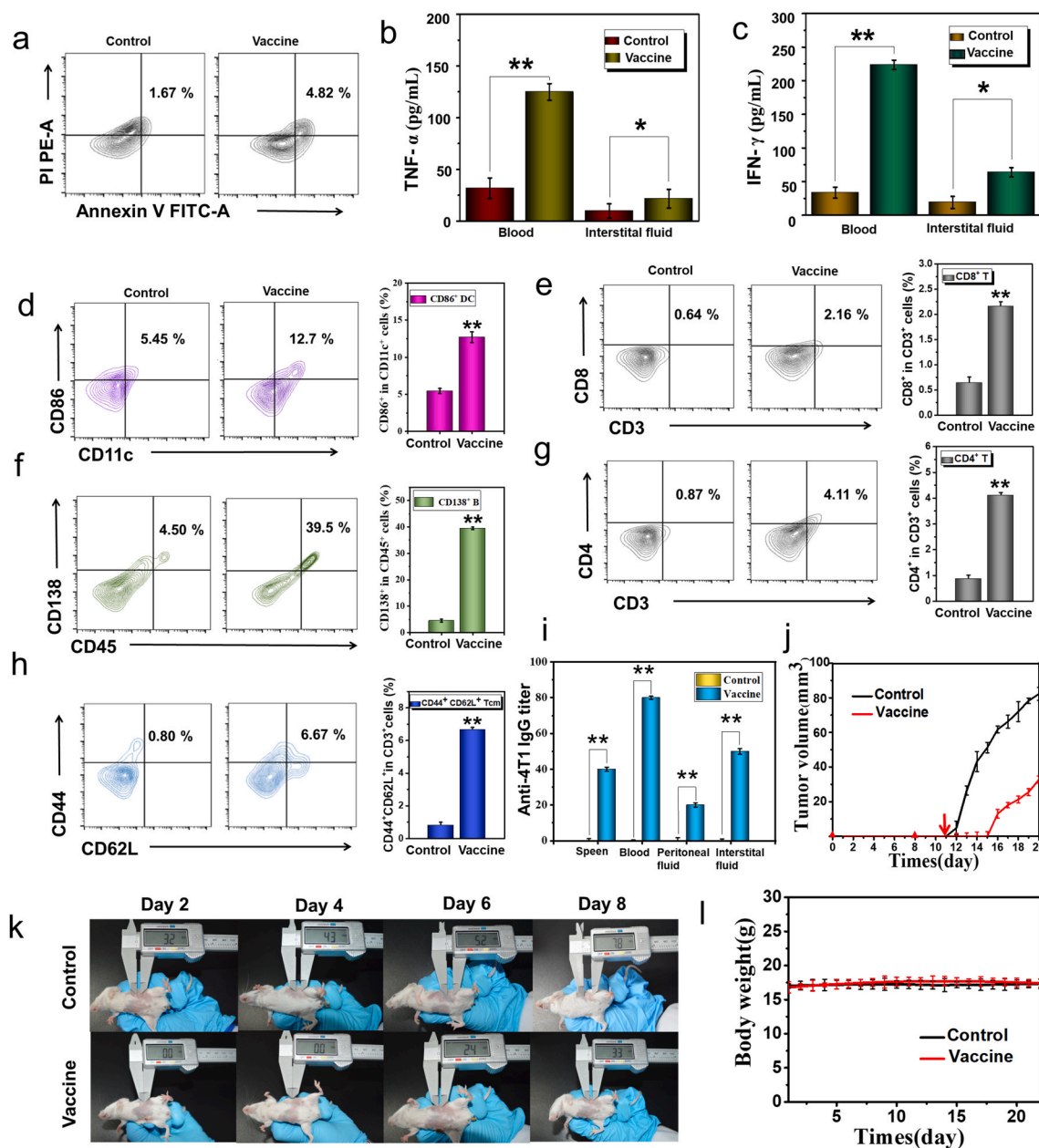
Fig. 7. SHV could suppress breast tumor in BLAB/c mice. (a) Analysis of apoptosis by flow cytometry in the injection site of mice after NIR irradiation (808 nm, 100 mW/cm^2, 10 min). (b, c) Secretion levels of TNF-α (b) and IFN-γ (c) in the blood and interstital fluid from immunized mice. (d) Activated DC ratio in inguinal lymph nodes for mice with different treatment (n = 3). APC anti-CD86 and PE anti-CD11c stained with CD86 and CD11c markers in DCs. (e) Cytotoxic T lymphocytes in interstitial fluid after treatment (n = 3). CD3 and CD8a as markers on CD8$^+$ T cell surfaces stained with APC anti-CD8a and FITC anti-CD3. Experiments were repeated three times. (f) Activated B cell ratio in bone marrows for mice with different treatment (n = 3). PE anti-CD138 and FITC anti-CD45 stained with CD138 and CD45 markers in B cells. (g) Helper T cells in interstitial fluid after treatment (n = 3). CD3 and CD4 as markers on CD4$^+$ T cell surfaces stained with Percp Cy5.5 anti-CD4 and FITC anti-CD3. Experiments were repeated three times. (h) Activated Central Memory T cell ratio in interstitial fluid for mice with different treatment (n = 3). PE anti-CD62L and APC anti-CD44 stained with CD62L and CD44 markers in Tcms. (i) Anti-4T1 IgG titer in spleen, blood, peritoneal fluid and interstitial fluid. (j) The growth curve of tumors in BLAB/c mice. (k) Representative photographs of tumors two weeks after injection of 4T1 cells in pre-immunized BLAB/c mice. (l) The body weight change curve of 4T1 tumor-bearing mice during the three weeks evaluation period. Statistical significance was calculated via one-way ANOVA with a Tukey post-hoc test (b, c, d, e, f, g, h, i and j), *P < 0.05; **P < 0.01; ***P < 0.001.

response to kill tumor cells.

Subsequently, we further explored the immune precaution of the SHV against tumor formation. It is well known that neutralizing antibody is the first barrier against foreign antigen, and it can clear tumor cells through antibody dependent cell-mediated cytotoxicity (ADCC). After immunization, the proportion of mature B cells secreting antibodies in bone marrow and spleen increased significantly (Fig. 7f and Fig. S51). At the same time, the titers of IgG against 4T1 cell surface antigen in spleen, blood, peritoneal fluid and interstitial fluid were detected by ELISA (Fig. 7i). The specific binding experiment of serum antibody of immunized mice to 4T1 cells also proved that the antibody activated by the vaccine can bind to the corresponding cell surface, further activate the immune function of the body, and play an anti-tumor role (Fig. S52). These results illustrated that the SHV successfully induced plasma cells to produce systemic specific antibodies against breast cancer cell antigens.

Cellular immunity is the most important way to eliminate tumor, so the formation of memory T cells is the key to the immune protection ability of vaccine. After immunizing BLAB/c mice twice, the Tcm cells in the lymph nodes were separated and analyzed by flow cytometry. The proportion of Tcm (CD44$^+$, CD62L$^+$) in lymph nodes of immunized mice increased nearly 10 times compared with the control group (Fig. 7h, Figs. S53 and S54). The above results suggested that the SHV could also successfully activate the systemic immune system of BLAB/c mice and form immune memory to prevent the invasion of breast cancer cells. Subsequently, 1×10^6 4T1 cells were inoculated into subcutaneous tissue of immunized mice to verify the protective effect of the vaccine. As shown in Fig. 7j and k, SHV significantly inhibited the growth of tumor. Meanwhile, the normal body weight changes of mice after vaccination showed that SHV had good biocompatibility (Fig. 7l). These results indicated that SHV was universal in inhibiting the occurrence of many kinds of tumors.

4. Conclusions

In order to improve the ability of immune adjuvants in anti-tumor vaccines to activate antigen-presenting cells (APCs), we constructed a SeV-based hydrogel vaccine (SHV) with non-pathogenic Sendai virus (SeV) as adjuvant. It can stimulate innate immune response in many ways for multi-channel recruitment and activation of dendritic cells (DCs). The thermosensitive hydrogel encapsulated tumor cells and the photosensitizer, which can be used for the NIR-control precise release of tumor antigens. All antigens of tumor cells were exposed under NIR irradiation and presented to lymph nodes effectively by surrounding DCs to induce the maturation of T lymphocytes and the formation of immune memory cells. The aOX40 in the vaccine could greatly improve the survival and expansion of effector T cells and memory T cells by binding to the OX40 ligand on the surface of T cells. Surprisingly, DNA fragments of tumor cells after photothermal damage could activate STING signaling pathway to improve the anti-tumor effect. In view of the presence of viruses in hydrogel vaccines, we had proved cautiously that viruses could not reproduce *in vivo*, did not cause acute infection, and did not lead to obvious histological changes. Meanwhile, the tumor cells that serve as antigen pools in the vaccine have no tumorigenicity after photothermal damage to release tumor antigen. The growth of B16 and 4T1 tumor was apparently inhibited by SHV. The vaccine had the advantages of simple preparation process, low cost and easy large-scale production. Theoretically, the B16 and 4T1 cells could be replaced with other antigens, such as other tumor cells, pathogenic microorganisms or individual antigen proteins, etc. In conclusion, the SHV system with excellent universality, convenience and flexibility might serve as the next generation of personalized anti-tumor vaccines, which represented an alternative way to suppress tumorigenesis.

CRediT authorship contribution statement

Bin Zheng: Conceptualization, Methodology, Validation, Writing – original draft, Investigation. **Wenchang Peng:** Data curation, Conceptualization, Writing – original draft, Formal analysis. **Lin Gan:** Supervision, Validation, Writing – review & editing. **Mingming Guo:** Resources, Data curation. **Shuchao Wang:** Validation, Data curation. **Xiao-Dong Zhang:** Data curation, Methodology. **Dong Ming:** Supervision, Funding acquisition.

Declaration of competing interest

The authors declare that they have no known competing financial interests or personal relationships that could have appeared to influence the work reported in this paper.

Acknowledgements

Appendix A. Supplementary data

Supplementary data to this article can be found online at https://doi.org/10.1016/j.bioactmat.2021.04.002.

Data availability statement

The data are available from the corresponding author on reasonable request.

References

[1] J.Y. Cai, H. Wang, D.G. Wang, Y.P. Li, Improving cancer vaccine efficiency by nanomedicine, Adv. Biosyst. 3 (3) (2019) 18.

[2] S. Li, X. Feng, J. Wang, W. Xu, M.A. Islam, T. Sun, Z. Xie, C. Wang, J. Ding, X. Chen, Multiantigenic nanoformulations activate anticancer immunity depending on size, Adv. Funct. Mater. 29 (49) (2019) 1429–1437.

[3] S. Shukla, M. Jandzinski, C. Wang, X. Gong, K.W. Bonk, R.A. Keri, N.F. Steinmetz, A viral nanoparticle cancer vaccine delays tumor progression and prolongs survival in a HER2(+) tumor mouse model, Advanced Therapeutics 2 (4) (2019) 4019–4028.

[4] Y.-W. Noh, S.-Y. Kim, J.-E. Kim, S. Kim, J. Ryu, I. Kim, E. Lee, S.H. Um, Y.T. Lim, Multifaceted immunomodulatory nanoliposomes: reshaping tumors into vaccines for enhanced cancer immunotherapy, Adv. Funct. Mater. 27 (8) (2017).

[5] M. Fusciello, F. Fontana, S. Tahtinen, C. Capasso, S. Feola, B. Martins, J. Chiaro, K. Peltonen, L. Ylosmaki, E. Ylosmaki, F. Hamdan, O.K. Kari, J. Ndika, H. Alenius, A. Urtti, J.T. Hirvonen, H.A. Santos, V. Cerullo, Artificially cloaked viral nanovaccine for cancer immunotherapy, Nat. Commun. 10 (2019) 5747.

[6] Z.-H. Huang, L. Shi, J.-W. Ma, Z.-Y. Sun, H. Cai, Y.-X. Chen, Y.-F. Zhao, Y.-M. Li, A totally synthetic, self-assembling, adjuvant-free MUC1 glycopeptide vaccine for cancer therapy, J. Am. Chem. Soc. 134 (21) (2012) 8730–8733.

[7] R.B. Patel, M. Ye, P.M. Carlson, A. Jaquish, L. Zangl, B. Ma, Y. Wang, I. Arthur, R. Xie, R.J. Brown, X. Wang, R. Sriramaneni, K. Kim, S. Gong, Z.S. Morris, Development of an in situ cancer vaccine via combinational radiation and bacterial-membrane-coated nanoparticles, Adv. Mater. 31 (43) (2019).

[8] J. Lv, C. Liu, H. Huang, L. Meng, B. Jiang, Y. Cao, Z. Zhou, T. She, L. Qu, S.W. Song, C. Shou, Suppression of breast tumor growth by DNA vaccination against phosphatase of regenerating liver 3, Gene Ther. 20 (8) (2013) 834–845.

[9] K. Aravindaram, P.H. Wang, S.Y. Yin, N.S. Yang, Tumor-associated antigen/IL-21-transduced dendritic cell vaccines enhance immunity and inhibit immunosuppressive cells in metastatic melanoma, Gene Ther. 21 (5) (2014) 457–467.

[10] D.N. Nguyen, J.J. Green, J.M. Chan, R. Longer, D.G. Anderson, Polymeric materials for gene delivery and DNA vaccination, Adv. Mater. 21 (8) (2009) 847–867.

[11] J. Li, Y. Sun, T. Jia, R. Zhang, K. Zhang, L. Wang, Messenger RNA vaccine based on recombinant MS2 virus-like particles against prostate cancer, Int. J. Canc. 135 (7) (2014) 1683–1694. E5.

[12] B.N. Hangalapura, L. Timares, D. Oosterhoff, R.J. Scheper, D.T. Curiel, T.D. de Gruijl, CD40-targeted adenoviral cancer vaccines: the long and winding road to the clinic, J. Gene Med. 14 (6) (2012) 416–427.

[13] S. Yamasaki, Y. Miura, J. Davydova, S.M. Vickers, M. Yamamoto, Intravenous genetic mesothelin vaccine based on human adenovirus 40 inhibits growth and metastasis of pancreatic cancer, Int. J. Canc. 133 (1) (2013) 88–97.

[14] B. Zheng, J. Xu, G. Chen, S. Zhang, Z. Xiao, W. Lu, Bacterium-mimicking vector with enhanced adjuvanticity for cancer immunotherapy and minimized toxicity, Adv. Funct. Mater. 29 (33) (2019).

[15] Z. Luo, Q. Wu, C. Yang, H. Wang, T. He, Y. Wang, Z. Wang, H. Chen, X. Li, C. Gong, Z. Yang, A Powerful CD8(+) T-cell stimulating D-tetra-peptide hydrogel as a very promising vaccine adjuvant, Adv. Mater. 29 (5) (2017).

[16] A.V. Kroll, R.H. Fang, Y. Jiang, J. Zhou, X. Wei, C.L. Yu, J. Gao, B.T. Luk, D. Dehaini, W. Gao, L. Zhang, Nanoparticulate delivery of cancer cell membrane elicits multiantigenic antitumor immunity, Adv. Mater. 29 (47) (2017).

[17] Y. Cao, Y. Ma, M. Zhang, H. Wang, X. Tu, H. Shen, J. Dai, H. Guo, Z. Zhang, Ultrasmall graphene oxide supported gold nanoparticles as adjuvants improve humoral and cellular immunity in mice, Adv. Funct. Mater. 24 (44) (2014) 6963–6971.

[18] H. Jiang, Q. Wang, L. Li, Q. Zeng, H. Li, T. Gong, Z. Zhang, X. Sun, Turning the old adjuvant from gel to nanoparticles to amplify CD8(+) T cell responses, Advanced Science 5 (1) (2018).

[19] Y.-W. Wu, M.-C. Chen, Y.-H. Chen, Potential zika vaccine: encapsulated nanocomplex promotes both T(H)1/T(H)2 responses in mice, Advanced Therapeutics 3 (3) (2020).

[20] A. Maeda, E. Digifico, F.T. Andon, A. Mantovani, P. Allavena, Poly(I:C) stimulation is superior than Imiquimod to induce the antitumoral functional profile of tumor-conditioned macrophages, Eur. J. Immunol. 49 (5) (2019) 801–811.

[21] L. Chen, L. Zhou, C. Wang, Y. Han, Y. Lu, J. Liu, X. Hu, T. Yao, Y. Lin, S. Liang, S. Shi, C. Dong, Tumor-targeted drug and CpG delivery system for phototherapy and docetaxel-enhanced immunotherapy with polarization toward M1-type macrophages on triple negative breast cancers, Adv. Mater. 31 (52) (2019).

[22] M. Glaffig, N. Stergiou, S. Hartmann, E. Schmitt, H. Kunz, A synthetic MUC1 anticancer vaccine containing mannose ligands for targeting macrophages and dendritic cells, ChemMedChem 13 (1) (2018) 25–29.

[23] Y. Xia, G.K. Gupta, A.P. Castano, P. Mroz, P. Avci, M.R. Hamblin, CpG oligodeoxynucleotide as immune adjuvant enhances photodynamic therapy response in murine metastatic breast cancer, J. Biophot. 7 (11–12) (2014) 897–905.

[24] B. Verstak, P. Hertzog, A. Mansell, Toll-like receptor signalling and the clinical benefits that lie within, Inflamm. Res. 56 (1) (2007) 1–10.

[25] C.V. Rosadini, J.C. Kagan, Early innate immune responses to bacterial LPS, Curr. Opin. Immunol. 44 (2017) 14–19.

[26] D. Paez-Espino, E.A. Eloe-Fadrosh, G.A. Pavlopoulos, A.D. Thomas, M. Huntemann, N. Mikhailova, E. Rubin, N.N. Ivanova, N.C. Kyrpides, Uncovering Earth's virome, Nature 536 (7617) (2016) 425–430.

[27] X. Dong, P. Pan, D.-W. Zheng, P. Bao, X. Zeng, X.-Z. Zhang, Bioinorganic hybrid bacteriophage for modulation of intestinal microbiota to remodel tumor-immune microenvironment against colorectal cancer, Science Advances 6 (20) (2020).

[28] D.-W. Zheng, X. Dong, P. Pan, K.-W. Chen, J.-X. Fan, S.-X. Cheng, X.-Z. Zhang, Phage-guided modulation of the gut microbiota of mouse models of colorectal cancer augments their responses to chemotherapy, Nature Biomedical Engineering 3 (9) (2019) 717–728.

[29] D.-W. Zheng, Y. Chen, Z.-H. Li, L. Xu, C.-X. Li, B. Li, J.-X. Fan, S.-X. Cheng, X.-Z. Zhang, Optically-controlled bacterial metabolite for cancer therapy, Nat. Commun. 9 (2018) 1680.

[30] K. Watanabe, Y.P. Luo, T. Da, S. Guedan, M. Ruella, J. Scholler, B. Keith, R.M. Young, B. Engels, S. Sorsa, M. Siurala, R. Havunen, S. Tahtinen, A. Hemminki, C.H. June, Pancreatic cancer therapy with combined mesothelin-redirected chimeric antigen receptor T cells and cytokine-armed oncolytic adenoviruses, JCI Insight 3 (7) (2018) 17.

[31] A. Kreso, C.A. O'Brien, P. van Galen, O.I. Gan, F. Notta, A.M.K. Brown, K. Ng, J. Ma, E. Wienholds, C. Dunant, A. Pollett, S. Gallinger, J. McPherson, C. G. Mulligan, D. Shibata, J.E. Dick, Variable clonal repopulation dynamics influence chemotherapy response in colorectal cancer, Science 339 (6119) (2013) 543–548.

[32] T.Z. Zhan, N. Rindtorff, J. Betge, M.P. Ebert, M. Boutros, CRISPR/Cas9 for cancer research and therapy, Semin. Canc. Biol. 55 (2019) 106–119.

[33] F.J. Sanchez-Rivera, T. Jacks, Applications of the CRISPR-Cas9 system in cancer biology, Nat. Rev. Canc. 15 (7) (2015) 387–395.

[34] T. Ura, K. Okuda, M. Shimada, Developments in viral vector-based vaccines, Vaccines 2 (3) (2014) 624–641.

[35] C.B. Lopez, B. Moltedo, L. Alexopoulou, L. Bonifaz, R.A. Flavell, T.M. Moran, TLR-independent induction of dendritic cell maturation and adaptive immunity by negative-strand RNA viruses, J. Immunol. 173 (11) (2004) 6882–6889.

[36] X. Mercado-Lopez, C.R. Cotter, W.-k. Kim, Y. Sun, L. Munoz, K. Tapia, C.B. Lopez, Highly immunostimulatory RNA derived from a Sendai virus defective viral genome, Vaccine 31 (48) (2013) 5713–5721.

[37] L.N. Liu, Y.H. Wang, L. Miao, Q. Liu, S. Musetti, J. Li, L. Huang, Combination Immunotherapy of MUC1 mRNA Nano-vaccine and CTLA-4 blockade effectively inhibits growth of triple negative breast cancer, Mol. Ther. 26 (1) (2018) 45–55.

[38] R. Yang, J. Xu, L.G. Xu, X.Q. Sun, Q. Chen, Y.H. Zhao, R. Peng, Z. Liu, Cancer cell membrane-coated adjuvant nanoparticles with mannose modification for effective anticancer vaccination, ACS Nano 12 (6) (2018) 5121–5129.

[39] Y. Tanaka, Z.J.J. Chen, STING specifies IRF3 phosphorylation by TBK1 in the cytosolic DNA signaling pathway, Sci. Signal. 5 (214) (2012) 11.

[40] D. Shae, K.W. Becker, P. Christov, D.S. Yun, A.K.R. Lytton-Jean, S. Sevimli, M. Ascano, M. Kelley, D.B. Johnson, J.M. Balko, J.T. Wilson, Endosomolytic polymersomes increase the activity of cyclic dinucleotide STING agonists to enhance cancer immunotherapy, Nat. Nanotechnol. 14 (3) (2019) 269–278.

[41] S.A. Ali, M. Ahmad, J. Lynam, C.S. McLean, C. Entwisle, P. Loudon, E. Choolun, S. E.B. McArdle, G. Li, S. Mian, R.C. Rees, Anti-tumour therapeutic efficacy of OX40L in murine tumour model, Vaccine 22 (27–28) (2004) 3585–3594.

[42] P. Bansal-Pakala, B.S. Halteman, M.H.Y. Cheng, M. Croft, Costimulation of CD8 T cell responses by OX40, J. Immunol. 172 (8) (2004) 4821–4825.

[43] F. Scaggs Huang, D.I. Bernstein, K.S. Slobod, A. Portner, T. Takimoto, C.J. Russell, M. Meagher, B.G. Jones, R.E. Sealy, C. Coleclough, K. Branum, M. Dickey, K. Buschle, M. McNeal, M. Makowski, A. Nakamura, J.L. Hurwitz, Safety and immunogenicity of an intranasal sendai virus-based vaccine for human parainfluenza virus type I and respiratory syncytial virus (SeVRSV) in adults, Hum. Vaccines Immunother. 17 (2) (2020) 554–559.

[44] M.L. Ge, Z. Luo, Z. Qiao, Y. Zhou, X. Cheng, Q.B. Geng, Y.Y. Cai, P. Wan, Y. Xiong, F. Liu, K.L. Wu, Y.L. Liu, J.G. Wu, HERP Binds TBK1 to activate innate immunity and repress virus replication in response to endoplasmic reticulum stress, J. Immunol. 199 (9) (2017) 3280–3292.

[45] J. Hiscott, Convergence of the NF-kappa B and IRF pathways in the regulation of the innate antiviral response, Cytokine Growth Factor Rev. 18 (5–6) (2007) 483–490.

[46] O.A. Ali, P. Tayalia, D. Shvartsman, S. Lewin, D.J. Mooney, Inflammatory cytokines presented from polymer matrices differentially generate and activate DCs in situ, Adv. Funct. Mater. 23 (36) (2013) 4621–4628.

[47] G. Zimmer, S. Bossow, L. Kolesnikova, M. Hinz, W.J. Neubert, G. Herrler, A chimeric respiratory syncytial virus fusion protein functionally replaces the F and HN glycoproteins in recombinant Sendai virus, J. Virol. 79 (16) (2005) 10467–10477.

[48] P.A. Bullough, F.M. Hughson, J.J. Skehel, D.C. Wiley, Structure of influenza haemagglutinin at the pH of membrane fusion, Nature 371 (6492) (1994) 37–43.

[49] A. Marcus, A.J. Mao, M. Lensink-Vasan, L. Wang, R.E. Vance, D.H. Raulet, Tumor-derived cGAMP Triggers a STING-mediated interferon response in non-tumor cells to activate the NK cell response, Immunity 49 (4) (2018) 754–763.

[50] J.M.T. Janco, P. Lamichhane, L. Karyampudi, K.L. Knutson, Tumor-infiltrating dendritic cells in cancer pathogenesis, J. Immunol. 194 (7) (2015) 2985–2991.

[51] J.P. Bottcher, C.R.E. Sousa, The role of type 1 conventional dendritic cells in cancer immunity, Trends Cancer 4 (11) (2018) 784–792.

[52] A. Gardner, B. Ruffell, Dendritic cells and cancer immunity, Trends Immunol. 37 (12) (2016) 855–865.

[53] S. Aspeslagh, S. Postel-Vinay, S. Rusakiewicz, J.C. Soria, L. Zitvogel, A. Marabelle, Rationale for anti-OX40 cancer immunotherapy, Eur. J. Canc. 52 (2016) 50–66.

[54] K.A. Murphy, M.G. Lechner, F.E. Popescu, J. Bedi, S.A. Decker, P.S. Hu, J. R. Erickson, M.G. O'Sullivan, L. Swier, A.M. Salazar, M.R. Olin, A.L. Epstein, J. R. Ohlfest, An in vivo immunotherapy screen of costimulatory molecules identifies Fc-OX40L as a potent reagent for the treatment of established murine gliomas, Clin. Canc. Res. 18 (17) (2012) 4657–4668.

[55] B.D. Curti, M. Kovacsovics-Bankowski, N. Morris, E. Walker, L. Chisholm, K. Floyd, J. Walker, I. Gonzalez, T. Meeuwsen, B.A. Fox, T. Moudgil, W. Miller, D. Haley, T. Coffey, B. Fisher, L. Delanty-Miller, N. Rymarchyk, T. Kelly, T. Crocenzi, E. Bernstein, R. Sanborn, W.J. Urba, A.D. Weinberg, OX40 is a potent immune-stimulating target in late-stage cancer patients, Canc. Res. 73 (24) (2013) 7189–7198.